Biosensors and Bioelectronics 127 (2019) 1–9

Contents lists available at ScienceDirect

Biosensors and Bioelectronics

journal homepage: www.elsevier.com/locate/bios

Chemical signals stimulate *Geobacter soli* biofilm formation and electroactivity

Xianyue Jing, Xing Liu, Chengsheng Deng, Shanshan Chen*, Shungui Zhou

Fujian Provincial Key Laboratory of Soil Environmental Health and Regulation, College of Resources and Environment, Fujian Agriculture and Forestry University, Fuzhou 350002, China

ARTICLE INFO

Keywords:
Geobacter soli
Chemical signal
Acylhomoserine lactone
Biofilm formation
Electroactivity

ABSTRACT

Biofilm formation and maturation have been demonstrated to be regulated by distinct forms of cell-cell communication factors such as chemical and physical signals. However, whether the *Geobacter* sp. biofilms, which are typical electroactive biofilms, are affected by chemical signals is poorly understood. This research investigated the effects and corresponding mechanisms of endogenous and exogenous chemical signals (i.e., N-acylhomoserine lactones, AHLs) on the *Geobacter soli* biofilm. The results showed that *Geobacter soli* GSS01 secreted detectable endogenous AHLs to facilitate the formation and electrochemical activity of the biofilm, and that exogenous AHLs could further promoted these activities. Analyses of surface proteins revealed that the mechanisms promoted by endogenous and exogenous AHLs were somewhat different. Endogenous AHLs improved the relative abundance of external membrane proteins, while exogenous AHLs further facilitated the formation of amide II and a stronger H-bond between the carbonyl group and the amide. Furthermore, the proteomics analysis indicated that endogenous AHLs enhanced extracellular polymeric substance production by up-regulating the expression of key enzymes participating in EPS production, and simultaneously affected the physiological performance of individual cells. These results demonstrate, for the first time, the importance of chemical signals in *Geobacter* sp. and provide a comprehensive understanding of the chemical signals involved in biofilm formation and electrochemical activity of *Geobacter* sp..

1. Introduction

Biofilms are widely applied in wastewater treatment systems since they grow on the solid surface and can easily be separated from water to avoid secondary pollution (Zhou et al., 2017). Electroactive biofilms (EABs) are one of the most promising types of biofilms for usage in wastewater treatment and other pollution control measures due to their unique capability of transferring electron to and from solid materials, such as electrodes. EABs play a key role in bioelectrochemical systems (BESs), which are devices capable of energy production, bioremediation, and value-added chemical production (Pant et al., 2012; Zhang et al., 2010; Choi and Sang, 2016), therefore, the formation and regulation of EABs are most crucial for BES performance (Zhuang et al., 2011).

Biofilm formation and maturation can be regulated by distinct forms of communication factors such as chemical signals (Lynch et al., 2002; Brameyer et al., 2015) and physical signals (Humphries et al., 2017). Quorum sensing (QS) is the best characterized cell-cell communication process in which bacteria employ chemical signals to enable communication that leads to synchronized collective behavior in a population density-dependent manner (Juhas et al., 2005; Ng and Bassler, 2009; Tseng et al., 2016). Generally, gram-negative bacteria employ the class of N-acylhomoserine lactones (AHLs) as chemical signals: thus, their QS system is called the AHL-dependent QS system (Brameyer et al., 2015). AHLs can be destroyed by acylases which hydrolyze the amide bond between the acyl chain and the homoserine lactone ring of AHLs (Utari et al., 2017).

Previous studies have documented that the QS system's influence on the performances of EABs in BESs. First, the QS system has a positive impact upon the electron shuttle production of *Pseudomonas aeruginosa*. For example, QS facilitates the production of phenazine, which acts as the electron shuttle to mediate electron transport from *P. aeruginosa* to the electrode (Venkataraman et al., 2010; W. Liu et al., 2015). Based on these studies, experiments were performed to manipulate the QS system of *P. aeruginosa*, such as overexpressing the QS *rhl* cassette or introducing a synthetic *pqsE* gene into a QS system negative mutant. These manipulations led to superior electron transfer capability (Yong et al., 2011; Wang et al., 2013). Second, AHLs regulate the microbial

* Corresponding author.
E-mail address: chenss@fafu.edu.cn (S. Chen).

https://doi.org/10.1016/j.bios.2018.11.051
Received 21 July 2018; Received in revised form 15 November 2018; Accepted 22 November 2018
Available online 07 December 2018
0956-5663/

community structure of mixed-culture EABs. Cai et al. (2016) reported that the cathodic microbial community structure in the presence of AHLs had more electrochemically active bacteria, which achieved a hydrogen yield increase of 81.82%. Chen et al. (2017) showed that the relative abundance of electroactive bacteria assigned to *Geoboacter* sp. increased with the addition of AHLs, resulting in the enhanced electrochemical activities of EABs. Third, AHLs play a role in biofilm formation. Monzon et al. (2016) added QS signals to *Halanaerobium praevalens* BESs and confirmed that exogenous alkyl-quinolones stimulated bacterial attachment to the anode but that exogenous AHLs could not. Chabert et al. (2018) demonstrated that exogenous AHLs improved the biofilm formation of *Acidithiobacillus ferrooxidans* on the electrode surface.

Whether the electrochemical activity and the biofilm formation of *Geobacter* sp. are influenced by AHLs, and whether *Geobacter* sp. generate endogenous AHLs, have not been reported. Previous works have shown that *Geobacter* sp. employs outer surface c-type cytochromes or conductive bacterial nanowires (Lovley, 2012; Reguera, 2011) in direct response to the electron-acceptor. Dong-yeon et al. (2017) defined this electron transfer of *Geobacter* sp. as electrochemical communication, and Reguera (2011) inferred that *Geobacter sulfurreducens* nanowires involved in cell–cell communication can be regarded as physical signals but not chemical signals, since physical signals can propagate through a wide range of media and enable rapid cellular responses. However, our previous study (Chen et al., 2017) showed that the relative abundance of *Geoboacter* sp. in EABs increased in response to exogenous AHLs, which suggests that *Geoboacter* sp. might be capable of receiving chemical signals. In addition, a homolog of QS gene *luxR* which codes for the AHL-receptor protein and a homolog of QS gene *luxI* which codes for the AHL-producer protein are found in *Geobacter soli* GSS01, *Geobacter sulfurreducens* PCA and *Geobacter metallireducens* GS-15 (Case et al., 2008). We thus hypothesize that both endogenous and exogenous chemical signals (AHLs) can affect the biofilm formation and properties of *Geobacter* sp. as well as the physical signals.

Geobacter soli GSS01was the first bacterium isolated from soil, has more environmentally significant physiological properties not found in *G. sulfurreducens*, and exhibit superior capacity for reducing insoluble Fe (III) oxides and generating current comparing with model species *G. sulfurreducens* PCA (Yang et al., 2017). Herein, to address the hypothesis, *Geobacter soli* GSS01 (Zhou et al., 2014) was inoculated into the pure-culture BES with different treatments. The main objectives of this study were to (i) investigate the positive impacts of endogenous and exogenous chemical signals on biofilm formation and electrochemical activity of *Geobacter soli* biofilms, and (ii) reveal the different stimulative mechanisms of endogenous and exogenous chemical signals by analyzing the outermost surface proteins and the whole suite of proteins via proteomics.

2. Materials and methods

2.1. Reactor construction and operation

The dual-chamber BES consisted of two cylindrical glass vessels with a liquid volume of 30 mL and a headspace volume of 5 mL. The chambers were separated by a proton exchange membrane (Nafion 117, DuPont Co., USA). Graphite plates (0.5 cm × 1 cm × 1.5 cm) were polished using sandpaper (grit type 400), sonicated for 30 min, soaked in 1 M HCl overnight, rinsed with Mili-Q water and then used as working and counter electrodes. The saturated calomel electrode (SCE) was used as the reference electrode and was connected to the working chamber with a porous vycor frit acting as salt bridge which prevented deviation of referential potential as previously described (Jana et al., 2014) (Fig. S1). The reactors were filled with deionized water, purged with N_2-CO_2 (80: 20), sealed with butyl-rubber stoppers (20 mm), and then autoclaved at 121 °C for 30 min. Then, the counter chamber was filled with anaerobic and sterile freshwater medium, while the working chamber was filled with anaerobic and sterile freshwater medium modified with 12 mM CH_3COONa as the electron donor. Two typical exogenous AHLs, N-Hexanoyl-DL-homoserine lactone (C6-HSL) and N-(3-oxo-dodecanoyl)-L-homoserine lactone (3OC12-HSL), were added to the working chamber to a final concentration of 10 μM. Acylase I (from porcine kidney) was added, with a final concentration of 6 μg/mL, to investigate the effect of endogenous AHLs. AHLs and/or acylase were added at each electric cycle. Control BESs (defined as CK) that received no AHL and acylase were also set up. *Geobacter soli* GSS01 was cultured as previously described (Zhou et al., 2014) and was inoculated into each working chamber after 50 mM phosphate buffer (PBS) washing and centrifugation. Working electrodes were polarized at 0.3 V vs. SCE with a multichannel potentiostat (CHI 1000 C, China), and current densities (mA/cm^2) were normalized with the maximum projected area of the working electrode (1.5 cm^2). Each treatment was run in fed-batch mode, at least quadruplicate, at 30 °C

2.2. Biofilm analysis

The structures of EABs were characterized using the LIVE/DEAD BacLight viability kit (L7012, Thermo Fisher Scientific, USA) and a confocal laser scanning microscope (CLSM) (LSM880, ZEISS, Germany) (Boulos et al., 1999). At least six CLSM images for each sample were selected at random. To evaluate the total biomass of EABs on the electrode, EABs were extracted with the protein extraction reagent with phenylmethanesulfonyl fluoride (PMSF) and DL-dithiothreitol (DTT) (One Step Bacterial Active Protein Extraction Kit, Sangon Biotech, China), and the bicinchoninic acid method (Smith et al., 1985) was used to determine the protein contents.

2.3. Electrochemical measurements

Cyclic voltammetry (CV) was performed with a workstation (CHI 660, Chenhua Instrument, China) in the range of 0.2 to −0.8 V at scan rates of 5 mV/s and 1 mV/s under turnover (in the presence of acetate) and non-turnover (in the absence of acetate) conditions in PBS, respectively. Electrochemical impedance spectroscopy (EIS) was conducted over a frequency range of 1000 kHz to 0.1 Hz, with a sinusoidal perturbation of 10 mV amplitude, to analyze the internal impedances of EABs. Extracellular polymeric substances (EPS) extraction was carried out as previously reported (Chen et al., 2017). The electron-accepting capacities (EAC) and electron-donating capacities (EDC) of EPS were detected in 0.1 M PBS and 0.1 M KCl as electrolyte that were purged with N_2 for 30 min before the measurements at applied potentials of −0.49 V and + 0.61 V, respectively, according to Yu et al. (2015).

2.4. Detection of AHLs

For AHLs detection, the electrolyte was collected after the biofilm had matured and was then centrifuged (5000 × *g* × 10 min). The supernatant was collected and extracted as previously described (Gould et al., 2006). The AHL-sensing bacterium *Agrobacterium tumefaciens* KYC55, with a β-galactosidase reporter gene and with sensitivity to a broad range of AHL derivatives, was provided by Prof. Jun Zhu (Nanjing Agricultural University, China) (Zhu et al., 2003) and was used to demonstrate the AHL secretion by *G. soli*. Analyses of AHLs using the reverse phase high-performance liquid chromatography (HPLC) coupled with ion trap mass spectrometry (Waters SQD 2, USA) were conducted according to Gould et al. (2006).

2.5. Outermost surface proteins and proteomics analysis

Electrochemical in situ Fourier transform infrared spectroscopy (FTIR) spectra were measured with a Nicolet 6700 FTIR spectrometer (Thermo Fisher Scientific) equipped with a liquid nitrogen-cooled, narrow-band MCT-A detector to observe the phase transition behavior

of the outermost surface proteins during electrochemical reactions. The glassy carbon electrode, the SCE and the Pt sheet were used as the working electrode, the reference electrode and the counter electrode, respectively. The working electrode was polished with 0.5 mm aluminum oxide powder before the biofilms were added onto its surface. A thin layer configuration equipped with a CaF_2 window was placed out of the IR chamber in a vertical configuration, and then the working electrode with biofilms was placed inside the IR cell, which was filled with 0.1 M PBS and 0.1 M KCl, during FTIR measurements. The sample potentials were set at a range of −0.8–0.4 V with an interval of 0.2 V, and the reference potential was set at −0.9 V. Two-dimensional correlation spectroscopy (2DCOS) was conducted, with potentials as the external perturbation, and were analyzed according to Chen et al. (2015).

Triple replicates of EABs with addition of AHLs or acylase, and the controls were harvested for protein extraction. In brief, the samples were incubated in lysis buffer (7 M Urea, 2 M Thiourea, 4% SDS, 40 mM Tris-HCl, and pH 8.5), containing 1 mM PMSF, 2 mM EDTA and 10 mM DTT, and were centrifuged to remove cell debris and to precipitate proteins. The proteins were mixed with acetone and centrifuged, and then the protein pellets were reduced, alkylated, digested and desalted. LC-ESI-MS/MS analysis was performed on a Triple TOF 5600 plus system. Data-dependent acquisition (DDA) was followed by SWATH acquisition for the same sample, with the same gradient conditions and the same amounts of sample. The original MS/MS data generated by DDA were submitted to ProteinPilot Software version 4.5 (AB Sciex, USA) for database searching. For protein identification, the Paragon algorithm (Shilov et al., 2007) integrated into ProteinPilot was employed. An automatic decoy database search strategy (Choi and Nesvizhskii, 2007) was employed to estimate the false discovery rate using the PSPEP (Proteomics System Performance Evaluation Pipeline Software, integrated in the ProteinPilot Software). Spectral library generation and SWATH data processing were performed using skyline (Sterling et al., 2013) version 3.5 software. Prior to targeted data extraction, a spectra library document was automatically generated. To eliminate the random errors and the sample bias, all the data were normalized using a median normalization method (Oberg and Mahoney, 2012). To assess the data confidence and to control the false discovery rate, the mProphet algorithm of skyline was employed towards each extracted peak.

3. Results and discussion

3.1. AHLs stimulate biofilm formation and electroactivity of Geobacter soli

Morphology and biomass were monitored throughout the first to the fifth cycles, demonstrating that both endogenous and exogenous AHLs stimulated biofilm formation of *Geobacter soli*. As shown in Fig. S2a and S2b, EABs with exogenous AHLs (including C6-HSL and 3OC12-HSL) had the most biomasses associated with anodes, but the biomass was obviously less without any AHL (i.e., the treatment with acylase addition). The CLSM images revealed the positive role of both endogenous and exogenous AHLs for biofilm formation. In the first cycle (Fig. 1), almost complete EABs appeared with exogenous AHLs, while other treatments did not. In the fifth cycle, visible mature biofilms were observed in Fig. 1 with exogenous AHLs, while only parts of the biofilms were metabolically active for other treatments. Moreover, AHLs significantly increased the ratio of live/dead cells and the shortness of the start-up period. Likewise, with acylase addition, the biomass and the biofilm formation were inferior to the controls, indicating that endogenous AHLs secreted by *G. soli* had the same function.

AHLs stimulated the electroactivity of *Geobacter soli* as well as the biofilm formation. Shortened start-up time and enhanced current outputs of BESs were obtained in the presence of AHLs (Fig. 2a). BESs with both exogenous and endogenous AHLs began to get pronounced current peaks at day 4, while BESs with only endogenous AHLs or without any AHLs attained initial current peaks at day 12 and day 20, respectively. In the fourth cycle, the maximum current density of the treatment without any AHL was lower than that with endogenous AHLs, both of which were just approximately half of the maximum current density in the presence of both exogenous and endogenous AHLs. In the first and second cycle, moreover, the current generation of per mg biomass was also enhanced in the presence of both exogenous and endogenous AHLs (Fig. S2c). To confirm the AHL-degradation function of acylase, treatments in the presence of both AHLs and acylase were also conducted. Additionally, AHLs or acylase applied in these experiments could not be used as carbon sources (Chen et al., 2017) nor could influence the growth of *G. soli* in liquid culture (Fig. S3), indicating that exogenous and endogenous AHLs play a regulative role in enhancing the current generation.

CV was employed to investigate the influence of AHLs on the redox activities of *G. soli* EABs. As depicted in CV under turnover conditions (Fig. 2b), *G. soli* EABs with exogenous AHLs attained the highest catalytic current among all the treatments. No redox peak was observed in the sterile PBS with the addition of AHLs and acylase (Fig. S4), indicating that all the redox signals were caused by biofilm-based redox compounds. CV under non-turnover conditions is shown in Fig. 2d. Three major redox systems with formal potentials of -0.39 ± 0.1 V (E_1), -0.29 ± 0.1 V (E_2) and -0.08 ± 0.1 V (E_3) can be distinguished for *G. soli* EABs with exogenous AHLs and the controls, and all these redox systems were involved in the bioelectrocatalytic electron transfer (Liu et al., 2008; Zhu et al., 2012). The redox peak located at E_2 disappeared with acylase addition, and all peak currents with exogenous AHLs were higher than those of the other treatments.

The EIS of EABs was used to reflect the processes of extracellular electron transfer involved in the overall electron transfer rate measured as current output (Babauta and Beyenal, 2017). As shown in Fig. 2c, all the EIS curves were fitted with equivalent circuits, which include solution resistance (R_s), charge transfer resistance (R_{ct}) and biofilm resistance ($R_{biofilm}$) as shown in the inset (Karthikeyan et al., 2015). BESs in the absence of endogenous and exogenous AHLs attained the highest R_{ct} and $R_{biofilm}$ among all the treatments. In contrast, the R_{ct} and $R_{biofilm}$ values upon exogenous AHLs addition were the lowest (Table S1), being about half of those from treatments with only endogenous AHLs, which highlights the effectiveness of both exogenous and exogenous AHLs in enhancing the charge transfer ability and electro-conductivities of *G. soli* EABs.

The EAC and EDC can be used to characterize the electroactivity of electrochemically active substances such as outer-membrane *c*-type cytochromes in EPS (Chen et al., 2017; Xiao et al., 2017). As shown in Fig. 3, the EAC of total EPS without endogenous AHLs was slightly lower than that of the controls. The EDC and EAC of the total EPS with the addition of C6-HSL were ~75% and ~50% higher than the controls, and the EDC of total EPS with 3OC12-HSL was ~50% higher than controls, demonstrating that exogenous AHLs could enhance the redox activities of EPS. Taken together, the results show that the CV and EIS as well as the EDC and EAC of EPS highlights that both endogenous and exogenous AHLs can improve the electrochemical activities of *G. soli* EABs.

3.2. Geobacter soli can secrete detectable AHLs

The formation and electroactivity of *G. soli* biofilm were inferior to the controls with acylase addition; thus, we speculated that *G. soli* secretes endogenous AHLs, and we conducted some experiments to confirm the AHL secretion. The AHL biosensor *Agrobacterium tumefaciens* KYC55 secreted β-galactosidase in the presence of AHLs, which hydrolyzed X-gal to generate macroscopic, colored small molecules. The KYC55 were cultured with the addition of extraction fractions to deduce whether *G. soli* EABs produced endogenous AHLs. As shown in Fig. 4, *G. soli* indeed secreted some endogenous AHLs. The types of endogenous AHLs secreted by *G. soli* were analyzed by LC/MS. Gould et al. (2006)

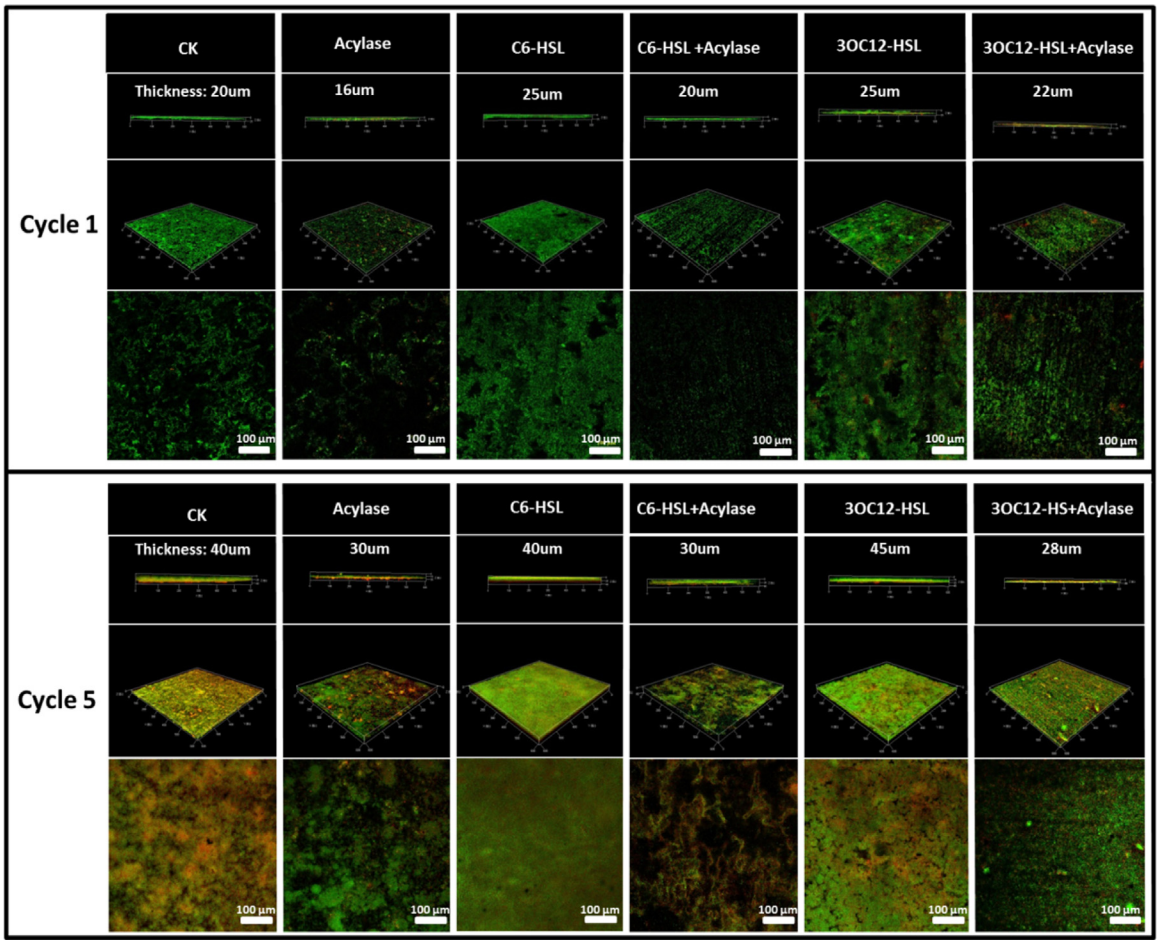

Fig. 1. CLSM Images with the addition of different AHLs and acylase for (a) the first and (b) the fifth cycles of the BESs. (Live cells were imaged as green, while dead cells were imaged as red.). (For interpretation of the references to color in this figure legend, the reader is referred to the web version of this article.)

showed the ions monitored in Q1 and Q3 of a series of AHL standards; thus, we followed the precursor ion-scanning analysis to identify AHLs in our samples. In this study, AHLs were detected in the electrolyte extract of *G. soli* by scanning for the parent ions shown in Fig. 4. The accurate masses at *m/z* 203.3 and their $[M + Na]^+$ adducts at *m/z* 303.3 were corresponded to 3OC5-HSL, 3OC14-HSL and C15-HSL, respectively (Gould et al., 2006). Therefore, we roughly inferred that *G. soli* could secrete one or several kinds of AHLs among 3OC5-HSL, 3OC14-HSL and C15-HSL.

3.3. Both exogenous and endogenous AHLs facilitate the formation of the outermost surface proteins

Molecules participating in the electron transport pathway to the cell exterior during the biofilm formation can be identified (Busalmen et al., 2010; Dong-yeon et al., 2017). The phase transition behaviors of outmost surface proteins during the biofilm formation were identified by electrochemical in situ FTIR spectroscopy which can reveal the electrochemical reaction of redox pairs at the molecular level. Bands that varied with potential shifting were related to redox reactions that occurred at cell-electrode interface (Yu et al., 2015). As shown in Fig. 5, bands appeared at 1158, 1250, 1400, 1418, 1523, 1600 and 1660 cm^{-1} for control biofilms (Fig. 5a), while there were only five bands at 1215 cm^{-1}, ~1350 cm^{-1}, 1478 cm^{-1}, 1553 cm^{-1} and 1660 cm^{-1} in the absence of endogenous AHLs (Fig. 5b). Comparing the spectra in Fig. 5a and b, the two major bands assigned to *c*-Cyts had one shifted one at 1215 cm^{-1}, suggesting a relatively lower abundance of external membrane proteins in the EABs without endogenous AHLs, and this should be the main reason for the lower current generation and the inferior biofilm in the absence of endogenous AHLs. As shown in Fig. 5c, the bands occurred at 1158, 1250, ~1350, 1418, 1540, 1600 and 1660 cm^{-1} for those with C6-HSL. Notably, the control biofilms (Fig. 5a) and those with exogenous AHLs were dominated by the strong absorbance bands at 1158 cm^{-1} and 1250 cm^{-1}, which were reported in relation to *c*-Cyts (Yang et al., 2017). Comparing the spectra depicted in Fig. 5a and c, the biofilm with exogenous AHLs lacked bands at 1400 cm^{-1} and 1513 cm^{-1}, which have been assigned to the amide III vibration of the peptide backbone and tyrosine (Busalmen et al., 2008; Ataka and Heberle, 2004); however, two new bands at ~1350 cm^{-1} and 1540 cm^{-1} appeared, which could be assigned to amide III and amide II. Amide II is a good indicator of the change in protein secondary structures (Yan et al., 2016) and Y. Liu et al. (2015) demonstrated that amide II loaded on external membranes proteins had the role of binding and electron transfer during biofilm formation. Thus, with the addition of exogenous AHLs, tyrosine was replaced by amide II which plays a key role in biofilm formation (Steenackers et al., 2012) and results in superior *G. soli* EABs.

In addition, 2DCOS was employed to enhance the spectral resolution of different outmost groups to various potentials. The synchronous maps showed two predominant autopeaks centered at 1250 cm^{-1} and 1612 cm^{-1} for the control (Fig. 5d), four centered at 1125 cm^{-1}, ~1350 cm^{-1}, 1478 cm^{-1} and 1612 cm^{-1} without endogenous AHLs (Fig. 5e), and two centered at ~1250 cm^{-1} and 1350 cm^{-1} in the presence of exogenous AHLs (Fig. 5f). Comparing the synchronous maps of Fig. 5d and f, the peaks correlating to 1612 cm^{-1} shifted to 1350 cm^{-1}. The lower wavenumber indicates a shorter atomic distance

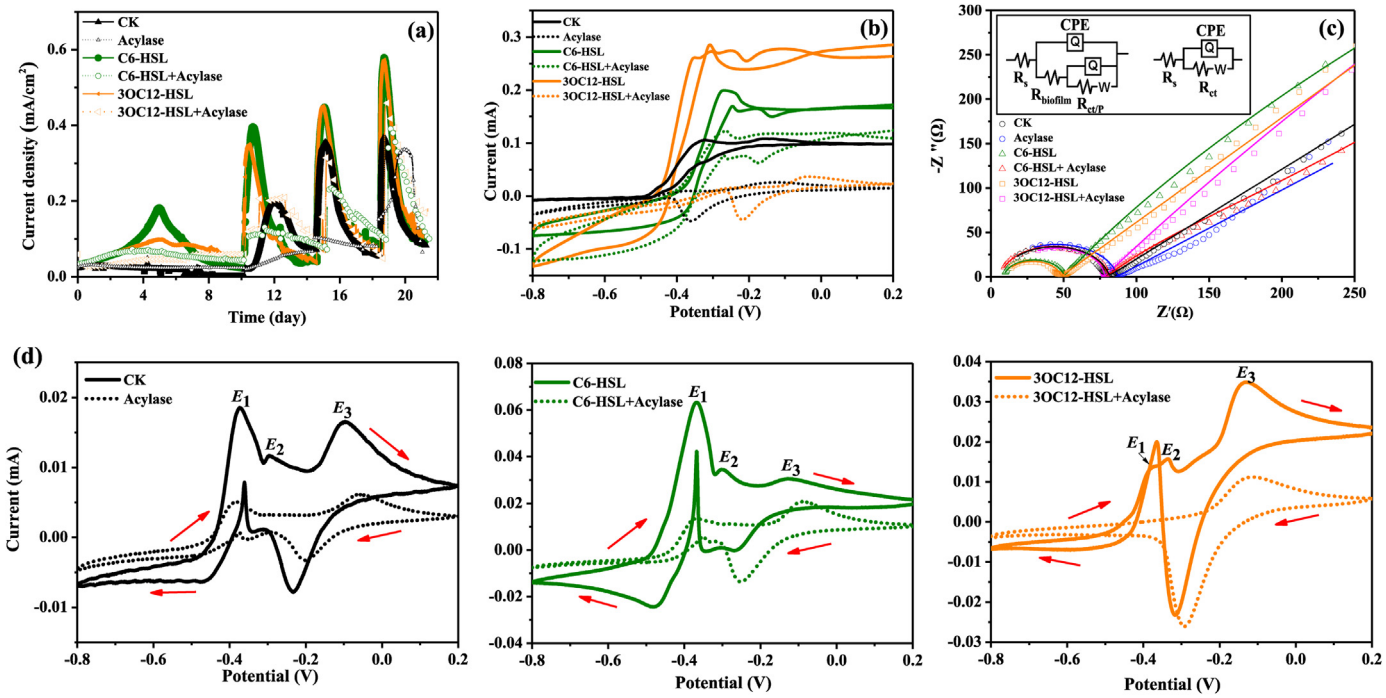

Fig. 2. Electrochemical performances of the EABs. (a) Current density produced versus time of the BESs for the five cycles with the addition of different AHLs (C6-HSL, 3OC12-HSL) or acylase (representative images are selected from three independent experiments), (b) cyclic voltammetric analyses of biofilm under the turnover condition (scan rates: 5 mV/s), (c) nyquist plots of BESs and the fitted data (solid line) according to the equivalent circuit (inserted), and (d) cyclic voltammetric analyses of biofilm under the non-turnover condition (scan rates: 1 mV/s) in presence of AHLs and/or acylase.

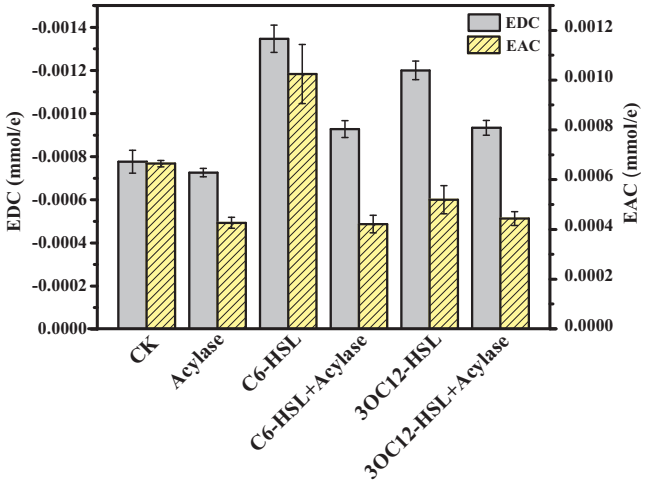

Fig. 3. EAC and EDC of the EPS in the presence of AHLs and/or acylase.

and a stronger protein H-bond (Jiang et al., 2010); thus, exogenous AHLs facilitated the formation of a stronger H-bond between the carbonyl group and the amide within the protein. The H-bonds of proteins at cell surfaces were more reactive in interfacial interactions than other functional groups (Yan et al., 2016), which could be a reason for the more electroactive biofilm formed with exogenous AHLs. The detailed assignments of the bands and the signs of their cross-peaks in asynchronous maps (Fig. 5g, h and i) are shown in Table 1. Using the sequential order rules in Chen et al. (2015), we inferred that the response rate change sequence of outmost groups to the shifting potentials (from −0.8 to 0.4 V) followed the following order: heme ring → amide III with exogenous AHLs. Without endogenous AHLs, the outmost groups followed the following order: binding of C-O stretching → binding of CH_2/CH_3 → amide III→ amide I. Previous studies indicated that there are many heme rings allocated in the outer membrane of the *Geobacter* EABs (Busalmen et al., 2008); however, the heme ring does not participate in the process of electron transfer in *G. soli* biofilm in the absence of endogenous AHLs. In general, endogenous AHLs improve the relative abundance of external membrane proteins, while with addition of exogenous AHLs further facilitate the formation of amide II and a stronger H-bond between the carbonyl group and amide in the *G. soli* biofilm.

3.4. Proposed mechanisms of AHL-effects on Geobacter soli biofilms revealed by comparative proteomics

The electrochemical experiments only reflect proteins involved in electron transfer, while proteomics of *G. soli* biofilms would further elucidate the multiple mechanisms of individual cells responding to AHLs. SWATH-MS is a recently advanced method that provides extensive lab-free quantitation of the peptide in a sample. Table S2 summarizes the number of the down-regulated ($p < 0.05$) and up-regulated ($p < 0.05$) proteins. COG and GO classifications of these proteins are shown in Fig. S5 and S6. SWATH-MS analysis revealed 445 proteins and 15 proteins with significantly different levels ($p < 0.05$) of abundance between pairwise comparisons of biofilms with endogenous and exogenous AHLs, respectively (Table S3 and S4). Among these proteins, 225 proteins and 7 proteins were up-regulated in the presence of endogenous and exogenous AHLs, respectively, while 170 proteins and 8 proteins with endogenous and exogenous AHLs, respectively, were down-regulated.

The differently expressed proteins were classified according to their COG categories (Fig. 6a and b). As shown in Fig. 6a, the COG of the biofilm exposed to acylase assessed the down-regulated proteins as involved in “energy production and conversion”, “nucleotide transport and metabolism”, “carbohydrate transport and metabolism” and “amino acid transport and metabolism”. Chen et al. (2003) revealed that endogenous AHLs secreted by *Sinorhizobium meliloti* influenced the expression levels of proteins involved in the above processes, consequently affecting biofilm formation, which is consistent with our

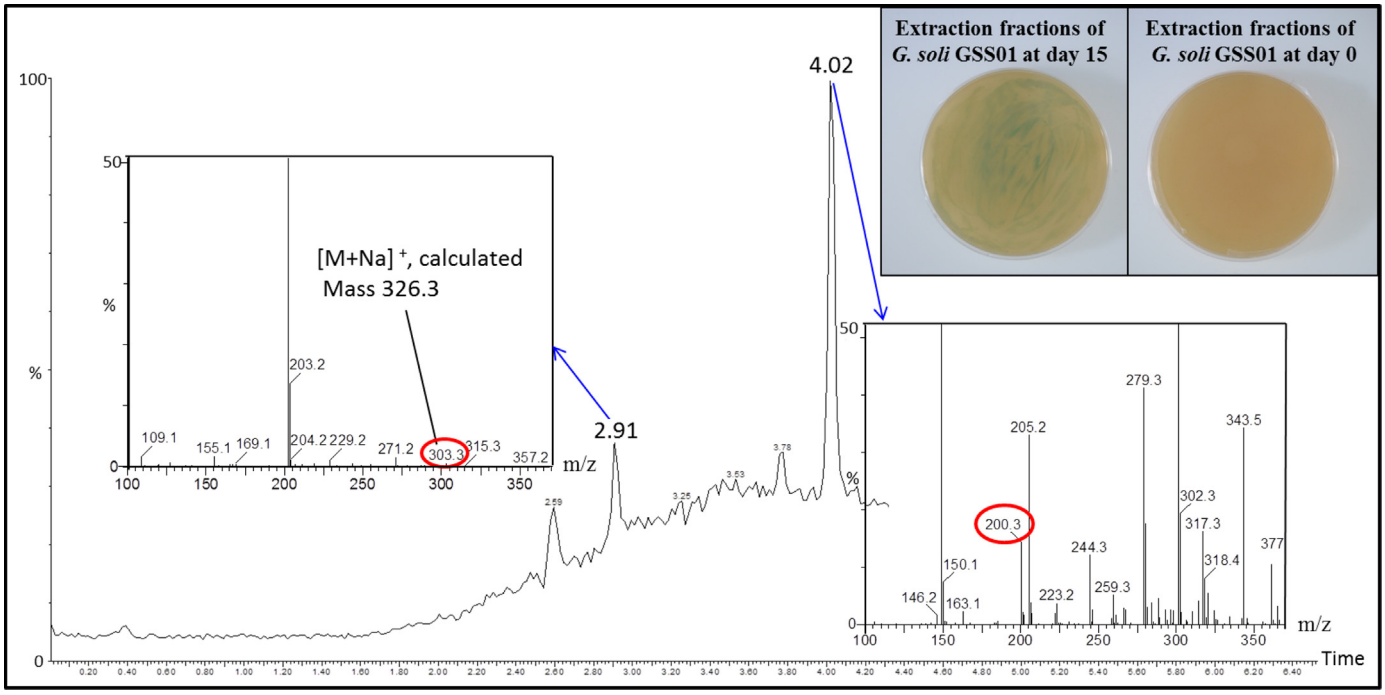

Fig. 4. Endogenous AHLs secreted by *Geobacter* soli GSS01 detected by (a) *Agrobacterium tumefaciens* strains KYC55 and (b) the mass spectrometry of AHLs produced by *Geobacter soli* GSS01.

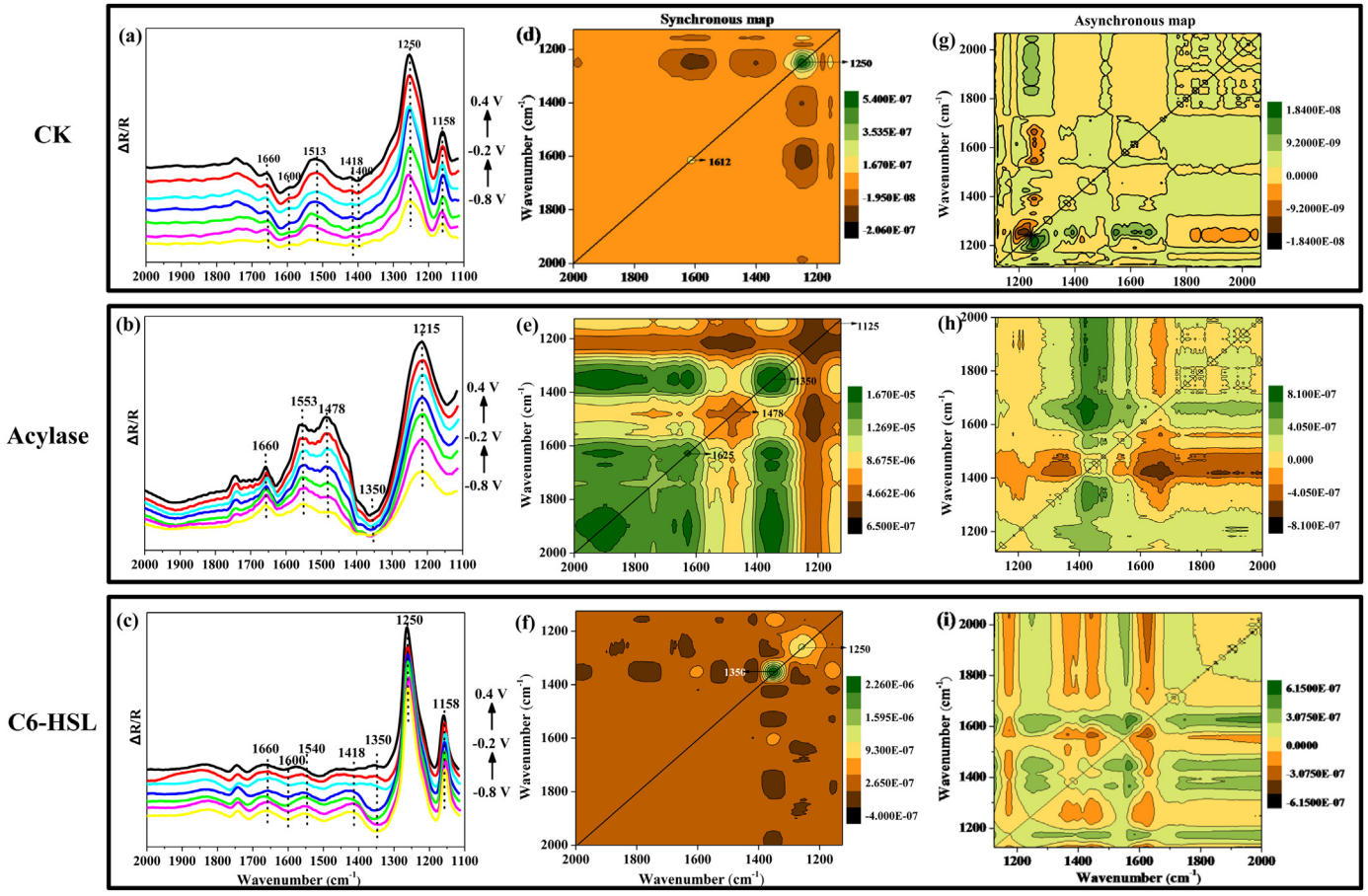

Fig. 5. (a) Electrochemical in situ FTIR spectra of living anode-associated *Geobacter soli* GSS01 biofilms with (b) acylase and (c) C6-HSL with varying potentials from −0.8 to 0.4 V. (d) Synchronous 2D correlation maps generated from FTIR analysis of anode-associated biofilms and (e) in the presence of acylase and (f) C6-HSL. (g) Asynchronous 2D correlation maps generated from FTIR analysis of anode-associated biofilms and (h) in presence of acylase and (i) C6-HSL.

Table 1
2D FTIR COS results on the assignment and sign of each cross-peak in synchronous and asynchronous maps of EABs with shifting potentials from −0.8 to 0.4 V.

	Position (cm^{-1})	Assignment	Sign[a]				The sequences of spectral change
CK			1250		1612		amide I → heme ring
	~1250	heme ring	+		- (-)		
	1612	amide I			+		
Acylase			1125	1350	1478	1625	C-O stretching → binding of CH_2/CH_3 → amide III → amide I
	1125	C-O stretching	+	+(+)	+(+)	+(+)	
	~1350	amide III		+	+(-)	+(+)	
	1478	binding of CH_2/CH_3			+	+(+)	
	1625	amide I				+	
C6-HSL			1250		1350		heme ring → amide III
	~1250	heme ring	+		+(+)		
	~1350	amide III			+		

[a] Signs were obtained in the upper-left corner of the maps: +, positive; -, negative.

results. Table S3 shows that, key enzymes participating in EPS production including phosphoenolpyruvate synthase, triosephosphate isomerase, glucose-6-phosphate isomerase as well as the phosphoglucomutase (Pirog et al., 2007; Velanker et al., 1997; Chignell et al., 2018; Degeest and Vuyst, 2000) were up-regulated 1.8-fold, 4.5-fold, 3.6-fold and 2-fold respectively in the presence of endogenous AHLs compared to those with acylase. Thus, the data demonstrates that endogenous AHLs may facilitate the expressing of key enzymes to improve EPS production. Moreover, many proteins related to metabolic processes, such as citrate synthase that plays a key role in the tricarboxylic acid (TCA) cycle (Table S3) (Bond et al., 2005) were down-regulated without endogenous AHLs, indicating that endogenous AHLs also influence the metabolic activity of *G. soli*. With exogenous AHL addition, NADH dehydrogenase, which is associated with electron transfer (Yu et al., 2018) was up-regulated 3-fold compared to the controls (Table S4), which could be a reason for the higher current density with exogenous AHLs addition. The above data shows that both endogenous and exogenous AHLs had obviously positive effects on the electroactivity of *G. soli* biofilms and the exogenous AHLs further effects on proteins expression of individual *G. soli* which induced the superior current generation of per mg biomass (Fig. S2c).

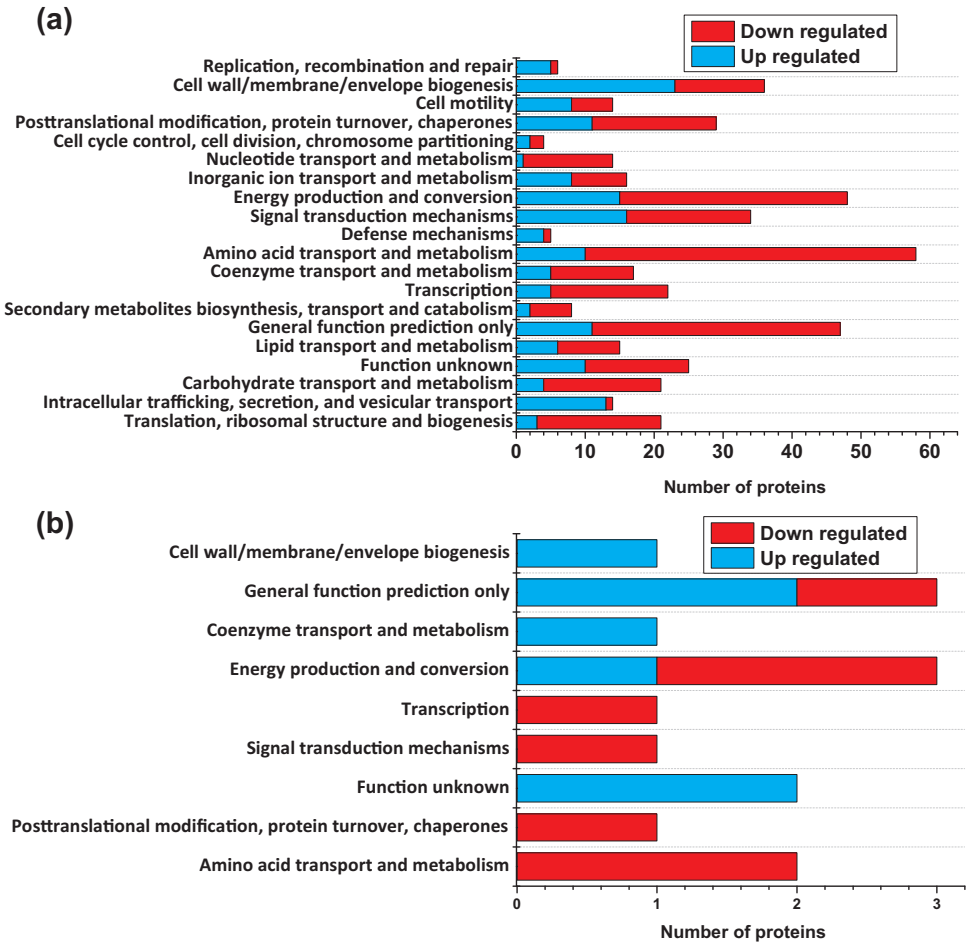

Fig. 6. Number of significantly differently expressed proteins ($p < 0.05$) with the addition of (a) acylase and (b) C6-HSL. The proteins were classified according to their COG categories.

4. Conclusions

In summary, *Geobacter soli* GSS01 biofilm with endogenous and exogenous AHLs shortened the star-up time by 12 days and increased the maximum current densities by 76% compared to biofilm without any AHL. *G. soli* secreted endogenous AHLs, which improved the relative abundance of external membrane proteins. Moreover, endogenous AHLs affect EPS formation by promoting the expression of the key enzymes participating in gluconeogenesis pathway. Additionally, endogenous AHLs play a critical role in physiological performance, including energy conversion, material transport and metabolism, of individual *G. soli* cells. Exogenous AHLs further facilitate the formation of amide II as well as a stronger H-bond between the carbonyl group and amide in the *G. soli* biofilm. Overall, the present work reveals the importance of chemical signals in *Geobacter* sp. and provides initial scientific evidence to reveal the stimulative mechanism of endogenous and exogenous AHLs.

Acknowledgments

Financial support was provided by the National Natural Science Foundation of China (Nos. 41501248 and 41877052), the Natural Science Foundation of Fujian Province (No. 2017J01653), and the Excellent Young Scientific Talent Incubation Program in Fujian Province University. We thank Prof. Jun Zhu at Nanjing Agricultural University for his kind provision of *Agrobacterium tumefaciens* KYC55, Zhongquan Lin at Fujian Agriculture and Forestry University for facilitating the CLSM analysis and the Wuhan GeneCreate Biological Engineering Co., Ltd. for proteomics analysis.

Appendix A. Supplementary material

Supplementary data associated with this article can be found in the online version at doi:10.1016/j.bios.2018.11.051.

References

Ataka, K., Heberle, J., 2004. Functional vibrational spectroscopy of a cytochrome *c* monolayer: seidas probes the interaction with different surface-modified electrodes. J. Am. Chem. Soc. 126, 9445–9457.
Babauta, J.T., Beyenal, H., 2017. Use of a small overpotential approximation to analyze *Geobacter sulfurreducens* biofilm impedance. J. Power Sources 356, 549–555.
Bond, D.R., Mester, T., Nesbø, C.L., Izquierdo-Lopez, A.V., Collart, F.L., Lovley, D.R., 2005. Characterization of citrate synthase from *Geobacter sulfurreducens* and evidence for a family of citrate synthases similar to those of eukaryotes throughout the *Geobacteraceae*. Appl. Environ. Microb. 71, 3858–3865.
Boulos, L., Prevost, M., Barbeau, B., Coallier, J., Desjardins, R., 1999. LIVE/DEAD® BacLight™: application of a new rapid staining method for direct enumeration of viable and total bacteria in drinking water. J. Microbiol. Methods 37, 77–86.
Brameyer, S., Bode, H.B., Heermann, R., 2015. Languages and dialects: bacterial communication beyond homoserine lactones. Trends Microbiol. 23, 521–523.
Busalmen, J.P., Esteve-Núñez, A., Berná, A., Feliu, J.M., 2008. C-type cytochromes wire electricity-producing bacteria to electrodes. Angew. Chem. 120, 4952–4955.
Busalmen, J.P., Esteve-Nuñez, A., Berná, A., Feliu, J.M., 2010. ATR-SEIRAs characterization of surface redox processes in *Geobacter sulfurreducens*. Bioelectrochemistry 78, 25–29.
Cai, W., Zhang, Z., Ren, G., Shen, Q., Hou, Y., Ma, A., Deng, Y., Wang, A., Liu, W., 2016. Quorum sensing alters the microbial community of electrode-respiring bacteria and hydrogen scavengers toward improving hydrogen yield in microbial electrolysis cells. Appl. Energy 183, 1133–1141.
Case, R.J., Maurizio, L., Staffan, K., 2008. AHL-driven quorum-sensing circuits: their frequency and function among the *Proteobacteria*. ISME J. 2, 345–349.
Chabert, N., Bonnefoy, V., Achouak, W., 2018. Quorum sensing improves current output with *Acidithiobacillus ferrooxidans*. Microb. Biotechnol. 11, 136–140.
Chen, H., Teplitski, M., Robinson, J.B., Rolfe, B.G., Bauer, W.D., 2003. Proteomic analysis of wild-type Sinorhizobium meliloti responses to N-acyl homoserine lactone quorum-sensing signals and the transition to stationary phase. J. Bacteriol. 185, 5029–5036.
Chen, S., Jing, X., Tang, J., Fang, Y., Zhou, S., 2017. Quorum sensing signals enhance the electrochemical activity and energy recovery of mixed-culture electroactive biofilms. Biosens. Bioelectron. 97, 369–376.
Chen, W., Habibul, N., Liu, X.Y., Sheng, G.P., Yu, H.Q., 2015. FTIR and synchronous fluorescence heterospectral two-dimensional correlation analyses on the binding characteristics of copper onto dissolved organic matter. Environ. Sci. Technol. 49, 2052–2058.
Chignell, J.F., Susan, K., Reardon, K.F., 2018. Meta-proteomic analysis of protein expression distinctive to electricity-generating biofilm communities in air-cathode microbial fuel cells. Biotechnol. Biofuels 11, 121.
Choi, H., Nesvizhskii, A.I., 2007. False discovery rates and related statistical concepts in mass spectrometry-based proteomics. J. Proteome Res. 7, 47–50.
Choi, O., Sang, B.I., 2016. Extracellular electron transfer from cathode to microbes: application for biofuel production. Biotechnol. Biofuels 9, 11.
Dong-yeon, D.L., Prindle, A., Liu, J., Süel, G.M., 2017. SnapShot: electrochemical communication in biofilms. Cell 170 (214-214).
Degeest, B., Vuyst, L.D., 2000. Correlation of activities of the enzymes α-phosphoglucomutase, UDP-galactose 4-epimerase and UDP-pyrophosphorylase with exopolysaccharide biosynthesis by *Streptococcus thermophilus* LY03. Appl. Environ. Microb. 66, 3519–3527.
Gould, T.A., Herman, J., Krank, J., Murphy, R.C., Churchill, M.E., 2006. Specificity of acyl-homoserine lactone synthases examined by mass spectrometry. J. Bacteriol. 188, 773–783.
Humphries, J., Xiong, L., Liu, J., Prindle, A., Yuan, F., Arjes, H.A., Tsimring, L., Süel, G.M., 2017. Species-independent attraction to biofilms through electrical signaling. Cell 168, 200–209.
Jana, P.S., Katuri, K., Kavanagh, P., Kumar, A., Leech, D., 2014. Charge transport in films of *Geobacter sulfurreducens* on graphite electrodes as a function of film thickness. Phys. Chem. Chem. Phys. 16, 9039–9046.
Jiang, W., Yang, K., Vachet, R.W., Xing, B., 2010. Interaction between oxide nanoparticles and biomolecules of the bacterial cell envelope as examined by infrared spectroscopy. Langmuir 26, 18071–18077.
Juhas, M., Eberl, L., Tümmler, B., 2005. Quorum sensing: the power of cooperation in the world of *Pseudomonas*. Environ. Microbiol. 7, 459–471.
Karthikeyan, R., Wang, B., Xuan, J., Wong, J.W., Lee, P.K., Leung, M.K., 2015. Interfacial electron transfer and bioelectrocatalysis of carbonized plant material as effective anode of microbial fuel cell. Electrochim. Acta 157, 314–323.
Liu, W., Cai, W., Ma, A., Ren, G., Li, Z., Zhuang, G., Wang, A., 2015. Improvement of bioelectrochemical property and energy recovery by acylhomoserine lactones (AHLs) in microbial electrolysis cells (MECs). J. Power Sources 284, 56–59.
Liu, Y., Berná, A., Climent, V., Feliu, J.M., 2015. Real-time monitoring of electrochemically active biofilm developing behavior on bioanode by using EQCM and ATR/FTIR. Sens. Actuators B-Chem. 209, 781–789.
Liu, Y., Harnisch, F., Fricke, K., Sietmann, R., Schröder, U., 2008. Improvement of the anodic bioelectrocatalytic activity of mixed culture biofilms by a simple consecutive electrochemical selection procedure. Biosens. Bioelectron. 24, 1006–1011.
Lovley, D.R., 2012. Electromicrobiology. Annu. Rev. Microbiol. 66, 391–409.
Lynch, M., 2002. The culture of control: Crime and social order in contemporary society. PoLAR: Political Leg. Anthropol. Rev. 25, 109–112.
Monzon, O., Yang, Y., Li, Q., Alvarez, P.J., 2016. Quorum sensing autoinducers enhance biofilm formation and power production in a hypersaline microbial fuel cell. Biochem. Eng. J. 109, 222–227.
Ng, W.L., Bassler, B.L., 2009. Bacterial quorum-sensing network architectures. Annu. Rev. Genet. 43, 197–222.
Oberg, A.L., Mahoney, D.W., 2012. Statistical methods for quantitative mass spectrometry proteomic experiments with labeling. BMC Bioinform. 13, 16.
Pant, D., Singh, A., Van Bogaert, G., Olsen, S.I., Nigam, P.S., Diels, L., Vanbroekhoven, K., 2012. Bioelectrochemical systems (BES) for sustainable energy production and product recovery from organic wastes and industrial wastewaters. RSC Adv. 2, 1248–1263.
Pirog, T.P., Vysyatetskaya, N.V., Korzh, Y.V., 2007. Specific features of the synthesis of the exopolysaccharide Ethapolan on a mixture of energy-deficient growth substrates. Microbiology 76, 25–30.
Reguera, G., 2011. When microbial conversations get physical. Trends Microbiol. 19, 105–113.
Shilov, I.V., Seymour, S.L., Patel, A.A., Loboda, A., Tang, W.H., Keating, S.P., Schaeffer, D.A., 2007. The Paragon Algorithm, a next generation search engine that uses sequence temperature values and feature probabilities to identify peptides from tandem mass spectra. Mol. Cell. Proteom. 6, 1638–1655.
Smith, P.K., Krohn, R.I., Hermanson, G.T., Mallia, A.K., Gartner, F.H., Provenzano, M., Fujimoto, E.K., Goeke, N.M., Olson, B.J., Klenk, D.C., 1985. Measurement of protein using bicinchoninic acid. Anal. Biochem. 150, 76–85.
Steenackers, H., Hermans, K., Vanderleyden, J., De Keersmaecker, S.C., 2012. *Salmonella* biofilms: an overview on occurrence, structure, regulation and eradication. Food Res. Int. 45, 502–531.
Sterling, C., Crouch, R., Russell, D.J., Calderón, A.I., 2013. ^{1}H NMR quantification of major saccharides in açaí raw materials: a comparison of the internal standard methodology with the absolute Intensity qNMR method. Phytochem. Anal. 24, 631–637.
Tseng, B.S., Majerczyk, C.D., da Silva, D.P., Chandler, J.R., Greenberg, E.P., Parsek, M.R., 2016. Quorum sensing influences *Burkholderia thailandensis* biofilm development and matrix production. J. Bacteriol. 198, 2643–2650.
Utari, P.D., Vogel, J., Quax, W.J., 2017. Deciphering physiological functions of AHL quorum quenching acylases. Front. Microbiol. 8, 1123.
Velanker, S.S., Ray, S.S., Gokhale, R.S., Suma, S., Balaram, H., Balaram, P., Murthy, M.R.N., 1997. Triosephosphate isomerase from *Plasmodium falciparum*: the crystal structure provides insights into antimalarial drug design. Structure 5, 751–761.
Venkataraman, A., Rosenbaum, M., Arends, J.B., Halitschke, R., Angenent, L.T., 2010. Quorum sensing regulates electric current generation of *Pseudomonas aeruginosa* PA14 in bioelectrochemical systems. Electrochem. Commun. 12, 459–462.
Wang, H., Ding, S., Wang, G., Xu, X., Zhou, G., 2013. In situ characterization and analysis of *Salmonella* biofilm formation under meat processing environments using a combined microscopic and spectroscopic approach. Int. J. Food Microbiol. 167, 293–302.

Xiao, Y., Zhang, E.H., Zhang, J.D., Dai, Y.F., Yang, Z.H., Christensen, H.E.M., Ulstrup, J., 2017. Extracellular polymeric substances are transient media for microbial extracellular electron transfer. Sci. Adv. 3, e1700623.
Yan, W., Wang, H., Jing, C., 2016. Adhesion of *Shewanella oneidensis* MR-1 to goethite: a two-dimensional correlation spectroscopic study. Environ. Sci. Technol. 50, 4343–4349.
Yang, G., Huang, L., You, L., Zhuang, L., Zhou, S., 2017. Electrochemical and spectroscopic insights into the mechanisms of bidirectional microbe-electrode electron transfer in *Geobacter soli* biofilms. Electrochem. Commun. 77, 93–97.
Yong, Y., Yu, Y., Li, C., Zhong, J., Song, H., 2011. Bioelectricity enhancement via overexpression of quorum sensing system in *Pseudomonas aeruginosa*-inoculated microbial fuel cells. Bioresour. Technol. 30, 87–92.
Yu, L., Yuan, Y., Chen, S., Zhuang, L., Zhou, S., 2015. Direct uptake of electrode electrons for autotrophic denitrification by *Thiobacillus denitrificans*. Electrochem. Commun. 60, 126–130.
Yu, L., Yuan, Y., Rensing, C., Zhou, S., 2018. Combined spectroelectrochemical and proteomic characterizations of bidirectional *Alcaligenes faecalis*-electrode electron transfer. Biosens. Bioelectron. 106, 21–28.
Zhang, X., Zhang, W., Xue, L., Zhang, B., Jin, M., Fu, Fu, 2010. Bioremediation of bacteria pollution using the marine sponge *Hymeniacidon perlevis* in the intensive mariculture water system of turbot *Scophthalmus maximus*. Biotechnol. Bioeng. 105, 59–68.
Zhou, S., Yang, G., Lu, Q., Wu, M., 2014. *Geobacter soli* sp. nov., a dissimilatory Fe(III)-reducing bacterium isolated from forest soil. Int. J. Syst. Evol. Microbiol. 64, 3786–3791.
Zhou, L., Li, T., An, J., Liao, C., Li, N., Wang, X., 2017. Subminimal inhibitory concentration (sub-MIC) of antibiotic induces electroactive biofilm formation in bioelectrochemical systems. Water Res. 125, 280–287.
Zhuang, L., Zhou, S., Yuan, Y., Liu, T., Wu, Z., Cheng, J., 2011. Development of Enterobacter aerogenes fuel cells: from in situ biohydrogen oxidization to direct electroactive biofilm. Bioresour. Technol. 102, 284–289.
Zhu, J., Chai, Y., Zhong, Z., Li, S., Winans, S.C., 2003. Agrobacterium bioassay strain for ultrasensitive detection of N-acylhomoserine lactone-type quorum-sensing molecules: detection of autoinducers in *Mesorhizobium huakuii*. Appl. Environ. Microb. 69, 6949–6953.
Zhu, X., Yates, M.D., Logan, B.E., 2012. Set potential regulation reveals additional oxidation peaks of *Geobacter sulfurreducens* anodic biofilms. Electrochem. Commun. 22, 116–119.